


# SCIENTIFIC REPORTS



OPEN

## Increase in resistance to anticancer drugs involves occludin in spheroid culture model of lung adenocarcinoma A549 cells

Hiroaki Eguchi<sup>1</sup>, Risa Akizuki<sup>1</sup>, Ryohei Maruhashi<sup>1</sup>, Mitsutoshi Tsukimoto<sup>2</sup>, Takumi Furuta<sup>3</sup>, Toshiyuki Matsunaga<sup>1</sup>, Satoshi Endo<sup>1</sup> & Akira Ikari<sup>1</sup> 

Chemoresistance is a serious issue in the therapy of many cancers, but the molecular mechanism is little understood. The mRNA level of occludin (OCLN), a tight junctional protein, was increased in the cisplatin (CDDP), doxorubicin (DXR), 7-ethyl-10-hydroxy-camptothecin, or gemcitabine-resistant human lung adenocarcinoma A549 cells. Here, we investigated the regulatory mechanism and pathophysiological role of OCLN. OCLN was mainly localized at tight junctions in A549 and CDDP-resistant A549 (A549/CDDP) cells. The level of p-Akt in A549/CDDP cells was higher than that in A549 cells, and the mRNA and protein levels of OCLN were suppressed by a phosphoinositide 3-kinase (PI3K)/Akt pathway inhibitor, LY-294002, suggesting that a PI3K/Akt pathway is involved in the elevation of OCLN expression. The overexpression of OCLN in A549 cells decreased paracellular permeability to DXR. Cytotoxicity to CDDP was unaffected by OCLN-overexpression in 2D culture model. In 3D culture model, the spheroid size, hypoxic level, and cell viability were significantly elevated by CDDP resistance, but not by OCLN-overexpression. The accumulation inside the spheroids and toxicity of DXR were correlated with OCLN expression. Our data suggest that OCLN is not directly involved in the chemoresistance, but it enhances chemoresistance mediated by suppression of accumulation of anticancer drugs inside the spheroids.

The pathology of lung cancer can be divided into non-small cell lung cancer (NSCLC) and small cell lung cancer. NSCLC accounts for approximately 80% of lung cancers diagnosed worldwide and contributes to poor survival<sup>1</sup>. NSCLC is classified as adenocarcinoma, squamous cell carcinoma, and large cell carcinoma. Among them, adenocarcinoma is the most popular type and shows little sensitivity to chemotherapy. Cisplatin (CDDP) is a platinum-based drug that is widely used in lung cancer treatment, but its effectiveness significantly decreases after the development of CDDP resistance. An acquired drug resistance can confer cross-resistance to diverse anticancer drugs, thereby causing inefficient treatment. Over 50% of patients undergoing lung cancer surgery acquire a chemoresistant phenotype<sup>2</sup>. Multiple mechanisms including induction of drug efflux pumps, anti-apoptosis factors, and drug-metabolizing enzymes are involved in the development of drug resistance<sup>3</sup>. The formation of tumor microenvironment is also involved in the development of chemoresistance<sup>4</sup>, but the molecular mechanism remain elusive.

Both malignant and non-malignant cells formed the tumor microenvironment *in vivo* during developing tumors. The inside cells of microenvironment experience severe stress conditions including hypoxia, oxidative stress, and so on<sup>5</sup>. Hypoxic stress causes adaptive responses such as the induction of genes transcription implicated in chemoresistance. A spheroid is a three-dimensional (3D) *in vitro* tumor model and resembles *in vivo* situation<sup>6</sup>. Cancer cells in 3D spheroid cultures often represent greater resistance to anticancer drugs than the cells grown in 2D monolayer cultures<sup>7</sup>. However, the molecular mechanisms of chemoresistance are not entirely elucidated in 3D culture model. We recently reported that claudin-1 (CLDN1) and CLDN2, components of tight junctions

<sup>1</sup>From the Laboratory of Biochemistry, Department of Biopharmaceutical Sciences, Gifu Pharmaceutical University, Gifu, Japan. <sup>2</sup>Department of Radiation Biosciences, Faculty of Pharmaceutical Sciences, Tokyo University of Science, Chiba, Japan. <sup>3</sup>Department of Pharmaceutical Chemistry, Kyoto Pharmaceutical University, Kyoto, Japan. Correspondence and requests for materials should be addressed to A.I. (email: [ikari@gifu-pu.ac.jp](mailto:ikari@gifu-pu.ac.jp))

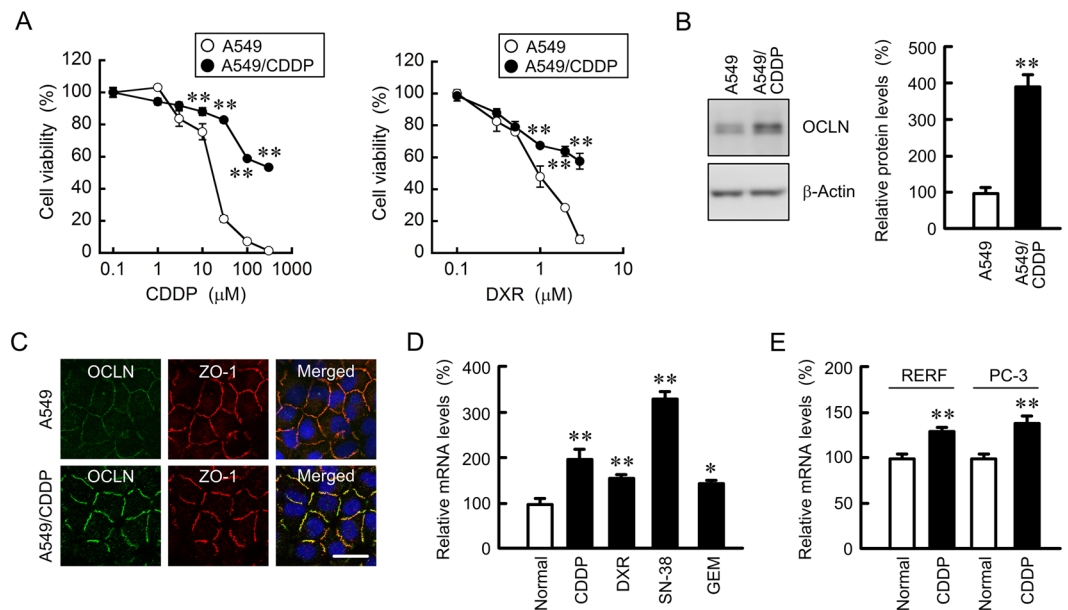


**Figure 1.** Elevation of mRNA level of *OCLN* in chemoresistant A549 cells. (A) A549 and A549/CDDP cells were cultured on a 96 well plate for 48 h followed by incubation with CDDP or DXR for additional 48 h at the concentrations indicated. Cell viability was measured by WST-1 assays. (B) The protein levels of *OCLN* and  $\beta$ -actin in cell lysates were examined by western blotting and shown as a percentage of the value in A549 cells. The full-length blot images are shown in Supplementary Fig. S1. (C) Immunofluorescence stainings with anti-*OCLN* (green) and anti-ZO-1 (red) antibodies were performed. The right images show the merged picture with DAPI (blue). Scale bar represents 10  $\mu$ m. (D) The expression levels of *OCLN* mRNA in anticancer drug-resistant cells are shown as a percentage of the values in parent cells (normal). (E) Total RNA was isolated from normal or CDDP-resistant RERF-LC-MS (RERF) and PC-3 cells. The expression levels of *OCLN* mRNA are shown as a percentage of the values in normal.  $n = 3-4$ . \*\* $P < 0.01$  and \* $P < 0.05$  compared with A549 or normal. NS,  $P > 0.05$ .

(TJs), decrease chemosensitivity to doxorubicin (DXR) in 3D-cultured A549 cells established from human lung adenocarcinoma<sup>8,9</sup>.

TJs regulate not only paracellular solute and ion transports, but also restrict the diffusion of membrane components<sup>10-12</sup>. In addition, TJs are involved in the coordination of cell differentiation, proliferation, and migration. Transmembrane proteins including occludin (*OCLN*), *CLDNs*, and junctional adhesion molecule exist in the bicellular TJs<sup>13,14</sup>. Tricellulin exists in the tricellular TJs of neighboring cells<sup>15</sup>. These proteins are scaffolded by zonula occludens (ZO)-1 that interacts with the actin cytoskeleton. *CLDNs* constitute a family with at least 24 different members in human and these subtypes can form homo- or heterophilic interactions between adjacent cells<sup>16,17</sup>. In contrast, *OCLN* is the first identified integral membrane protein of TJs and has no subtype<sup>18</sup>. In the respiratory system, *OCLN* is expressed in bronchial airway and alveolar cells under physiological conditions<sup>19,20</sup>. In an immunohistochemical analysis, *OCLN* is expressed in human lung adenocarcinomas, but not in squamous cell carcinomas and large cell carcinomas<sup>21</sup>. In addition, the mRNA level of *OCLN* is increased in adenocarcinomas compared to normal lung tissue<sup>22</sup>. However, the pathophysiological role of *OCLN* in lung adenocarcinoma tissue has not been clarified yet.

The expression level of *OCLN* in CDDP-resistant A549 (A549/CDDP) cells was higher than that in parent A549 cells. Therefore, we investigated the regulatory mechanism and pathophysiological role of *OCLN* expression. The elevation of mRNA and protein levels of *OCLN* was inhibited by a phosphoinositide 3-kinase (PI3K) inhibitor, LY-294002, in A549/CDDP cells. Cytotoxicity to DXR was not changed by *OCLN*-overexpression in 2D culture model, but paracellular permeability to DXR was decreased. Additionally, *OCLN* overexpression decreased the accumulation and cytotoxicity of DXR in 3D culture model. These results indicate that *OCLN* may be implicated in the promotion of chemoresistance in A549 spheroid cells.

## Results

### Effect of resistance to anticancer drugs on the expression and localization of *OCLN* in A549 cells.

CDDP, an anticancer drug containing platinum, concentration-dependently increased toxicity of A549 cells (Fig. 1A). Compared with the parent cells, the chemosensitivity to CDDP was significantly lower at above 10  $\mu$ M in A549/CDDP cells. In addition, the sensitivity to DXR was also attenuated by developing the CDDP resistance, indicating that A549/CDDP cells acquired cross resistance to DXR. The protein level of *OCLN* in A549/CDDP cells was significantly higher than that in A549 cells (Fig. 1B). Immunofluorescence measurements showed that *OCLN* was mainly colocalized with ZO-1 and DAPI, indicating that *OCLN* are distributed in the TJs (Fig. 1C). The CDDP resistance increased the fluorescence intensity of *OCLN* at the TJs in A549/CDDP cells, but it did not change the intracellular localization of *OCLN*. The mRNA level of *OCLN* in A549/CDDP cells is higher

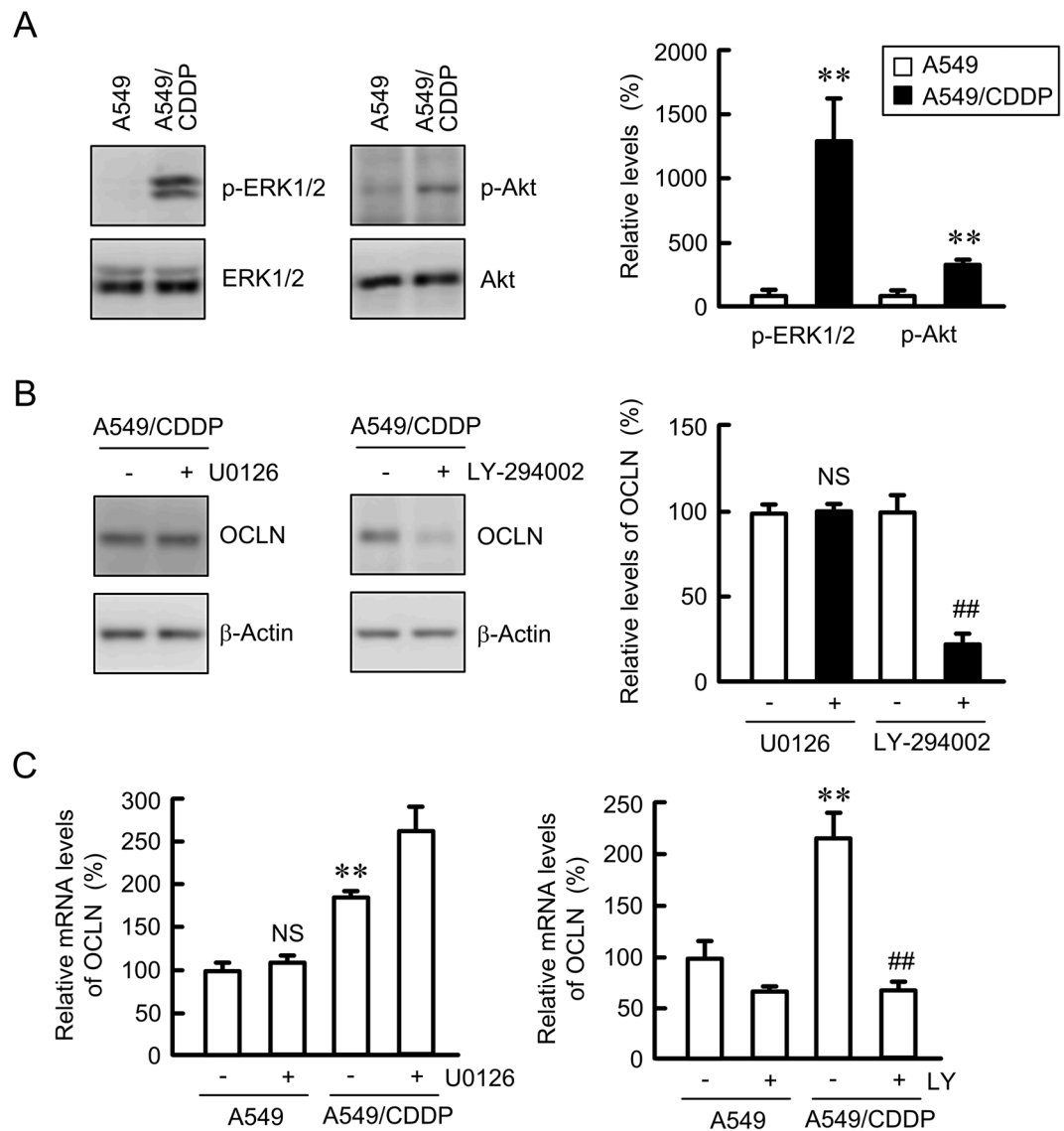


**Figure 2.** Decrease in OCLN expression by LY-294002 in A549/CDDP cells. **(A)** The expression of p-ERK1/2, ERK1/2, p-Akt, and Akt in whole cell extracts was examined by western blotting. The levels of p-ERK1/2 and p-Akt are shown as a percentage of the values in A549 cells. The full-length blot images are shown in Supplementary Fig. S2A. **(B)** A549/CDDP cells were treated with or without 10  $\mu$ M U0126 and 10  $\mu$ M LY-294002 for 24 h. The expression of OCLN and  $\beta$ -actin in cell lysates was examined by western blotting. The protein levels of OCLN are shown as a percentage of the values in the absence of inhibitor. The full-length blot images are shown in Supplementary Fig. S2B. **(C)** A549 and A549/CDDP cells were treated with or without U0126 and LY-294002 for 6 h. The expression levels of OCLN mRNA are shown as a percentage of the values in the absence of inhibitor.  $n = 3-4$ . \*\* $P < 0.01$  compared with A549. ## $P < 0.01$  compared with -LY. NS,  $P > 0.05$  compared with -U0126.

than that in normal cells (Fig. 1D), indicating that CDDP resistance increases OCLN expression at the transcriptional step. Similarly, the mRNA level of *OCLN* was increased by resistance to DXR, gemcitabine (GEM), and 7-ethyl-10-hydroxy-camptothecin (SN-38), a metabolite of the camptothecin derivative CPT-11, in A549 cells. In addition, that of *OCLN* was increased by resistance to CDDP in human lung adenocarcinoma RERF-LC-MS and PC-3 cells (Fig. 1E). These results indicated that the resistance to anticancer drugs increased the expression and tight junctional localization of OCLN in A549 cells.

**Elevation of OCLN expression by phosphoinositide 3-kinase (PI3K)/Akt signaling pathway in A549/CDDP cells.** To clarify the mechanism of OCLN upregulation by CDDP resistance, we investigated the involvement of mitogen-activated protein kinase kinase (MEK)/ extracellular signal-regulated kinase (ERK) and PI3K/Akt signaling pathways. The p-ERK1/2 and p-Akt levels in A549/CDDP cells were significantly higher than those in the parent cells (Fig. 2A). In contrast, there is no difference in the total levels of ERK1/2 and Akt. The protein level of OCLN was suppressed by LY-294002 in A549/CDDP cells, but not by U0126, a MEK/ERK

pathway inhibitor (Fig. 2B). Similarly, the CDDP resistance-induced elevation of OCLN mRNA was suppressed by LY-294002 (Fig. 2C). In contrast, U0126 increased the level of OCLN mRNA in A549/CDDP cells. These results indicated that PI3K/Akt pathway may be involved in the elevation of OCLN expression in A549/CDDP cells.

**Effects of CDDP resistance and OCLN overexpression on paracellular permeability.** CDDP resistance did not change transepithelial electrical resistance (TER) in A549 cells, but inhibited the paracellular permeability to DXR (Fig. 3A). Similarly, LY-294002 did not change TER in A549/CDDP cells, but it enhanced paracellular DXR flux (Fig. 3B). To clarify the involvement of OCLN in the regulation of TJ properties, we established stably OCLN-expressing A549 cells (OCLN/A549). The expression of OCLN was confirmed by western blotting using anti-FLAG and anti-OCLN antibodies (Fig. 3C). The overexpression of OCLN inhibited paracellular DXR flux without affecting TER (Fig. 3D). These results were similar to those in A549/CDDP cells.

**Effect of OCLN overexpression on toxicity against anticancer drugs in A549 cells.** The toxicity against anticancer drugs was estimated in 2D monolayer culture of A549 cells. Both CDDP and DXR dose-dependently increased cytotoxicity (Fig. 4A). The overexpression of OCLN did not affect the toxicity against anticancer drugs. In western blotting and quantitative real time polymerase chain reaction (PCR) analyses, both protein and mRNA levels of ATP-binding cassette (ABC) transporters, including ABCB1, ABCC1, ABCC2, and ABCG2 were not changed by OCLN overexpression (Fig. 4B,C). These results indicated that OCLN may not be directly involved in the chemoresistance in 2D culture model.

**Effect of CDDP resistance on formation of spheroids.** A549 cells form spheroids by culturing in round-bottom 96-well plates. A549/CDDP cells showed larger size of spheroids than A549 cells (Fig. 5A). The hypoxic level and cell viability in A549/CDDP cells were higher than those in A549 cells (Fig. 5B,C). In immunofluorescence measurement of spheroid cells showed that both OCLN and ZO-1 were distributed in the cell-cell border area of most outside cells (Fig. 5D). These results indicated that CDDP resistance may enhance viability and hypotonic stress in spheroid cells.

**Effect of OCLN overexpression on formation of spheroids.** As described above, the size of spheroid in A549/CDDP cells was larger than that in A549 cells, but OCLN overexpression did not change the size (Fig. 6A). In addition, OCLN overexpression had no effect on hypoxic level (Fig. 6B) and cell viability (Fig. 6C). These results indicated that the phenomena of OCLN overexpressing cells are not incompletely matched with those of A549/CDDP cells. OCLN may not be directly implicated in the growth of spheroids.

**Elevation of chemoresistance spheroid cells by OCLN overexpression.** The fluorescence intensity of DXR in the spheroids dose-dependently elevated in A549 cells, indicating that DXR was accumulated in the spheroids (Fig. 7A). The accumulation of DXR was significantly inhibited by CDDP resistance and OCLN overexpression. DXR dose-dependently decreased the size and viability in spheroid cells (Fig. 7B,C), which were recovered by CDDP resistance and OCLN overexpression. These results indicated that OCLN overexpression may enhance chemoresistance in spheroid cells.

**Effect of OCLN siRNA on paracellular permeability to DXR and cytotoxicity.** Next, the effect of OCLN siRNA on paracellular DXR permeability was examined in 2D model and on DXR-induced chemoresistance in A549/CDDP spheroid cells. The protein level of OCLN was decreased over 60% by OCLN siRNA in A549/CDDP cells (Fig. 8A). The introduction of OCLN siRNA in A549/CDDP cells increased paracellular permeability to DXR (Fig. 8B). In contrast, TER was unchanged by OCLN knockdown (Fig. 8C). Neither spheroid size nor hypoxic level were changed by OCLN siRNA (Fig. 8D,E). The accumulation and toxicity of DXR in A549/CDDP cells were increased by OCLN siRNA (Fig. 8F,G). These results show an inverse relationship of OCLN expression with CDDP sensitivity, indicating that the increase in OCLN expression may be implicated in reducing chemosensitivity of A549/CDDP spheroid cells.

**Increase in CDDP and SN-38 toxicities of A549/CDDP spheroid cells by OCLN siRNA.** As shown above, OCLN siRNA significantly enhanced DXR toxicity in A549/CDDP cells. To clarify the effects of other anticancer drugs toxicities, we examined the effect of CDDP and SN-38 toxicities in A549/CDDP spheroid cells. Both CDDP and SN-38 dose-dependently decreased the spheroid size and cell viability, which were exaggerated by OCLN siRNA (Fig. 9). The effect of OCLN knockdown on CDDP and SN-38 toxicities agree with that on DXR toxicity. These results indicated that the elevation of OCLN expression in spheroids may cause resistance to lung cancer chemotherapy.

## Discussion

A549/CDDP cells acquired resistance to not only CDDP, but also DXR (Fig. 1A). Similarly, cross resistance to anticancer drugs are reported in docetaxel-resistant<sup>23</sup> and gemcitabine-resistant A549 cells<sup>24</sup>. The detailed mechanism of acquisition of chemoresistance has not been fully understood. In the present study, we found for the first time that OCLN expression is elevated in anticancer drug-resistant A549 cells (Fig. 1). Similarly, the increase in OCLN mRNA was also observed in CDDP-resistant RERF-LC-MS and PC-3 cells, indicating that the induction of OCLN may commonly occur in chemoresistant lung adenocarcinoma cells. Furthermore, OCLN may affect the function of TJs because the induced OCLN is localized at the TJs.

So far, the activation of ERK1/2 and Akt pathways, two major cell survival pathways, has been reported in CDDP-resistant gastric cancer cells<sup>25</sup> and ovarian cancer cells<sup>26</sup>. The inhibition of ERK1/2 or Akt pathway re-sensitizes the resistant cells to CDDP. Similarly, our data indicated that the levels of p-ERK1/2 and p-Akt in

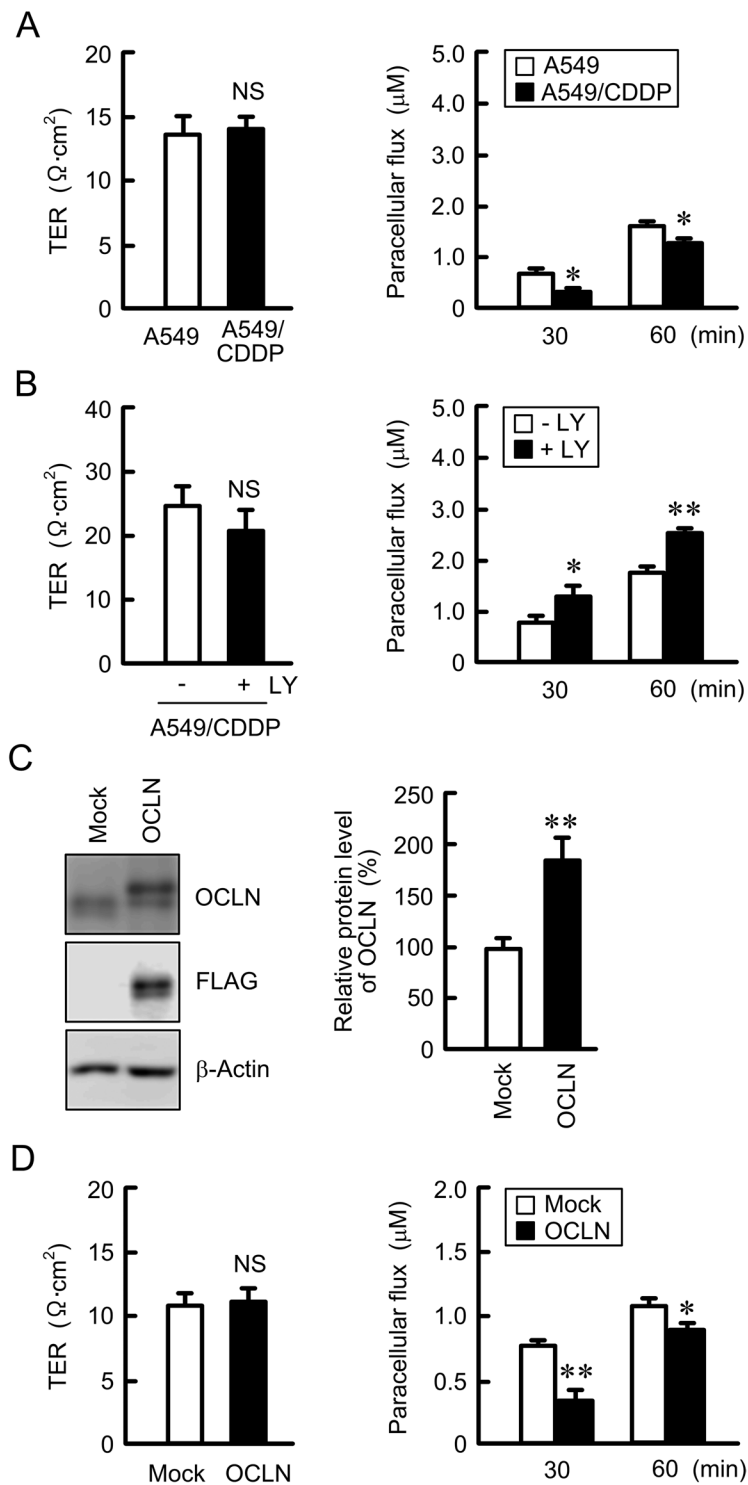


**Figure 3.** Effect of OCLN expression on tight junction permeability. (**A** and **B**) A549 and A549/CDDP cells were plated on transwell inserts. As indicated, A549/CDDP cells were treated with or without of 10  $\mu\text{M}$  LY-294002 (LY) for 24 h. TER and paracellular DXR flux were analyzed by a volt ohmmeter and fluorescence spectrometry, respectively. (**C**) Cell lysates were prepared from empty (mock) or FLAG-tagged OCLN-expressing cells. The expression of OCLN, FLAG, and  $\beta$ -actin was examined by western blotting. The protein levels of OCLN are shown as a percentage of the values in mock cells. The full-length blot images are shown in Supplementary Fig. S3. (**D**) TER and the paracellular DXR flux were measured in mock and OCLN-expressing cells.  $n = 3-4$ . \*\* $P < 0.01$  and \* $P < 0.05$  compared with A549. NS,  $P > 0.05$ .

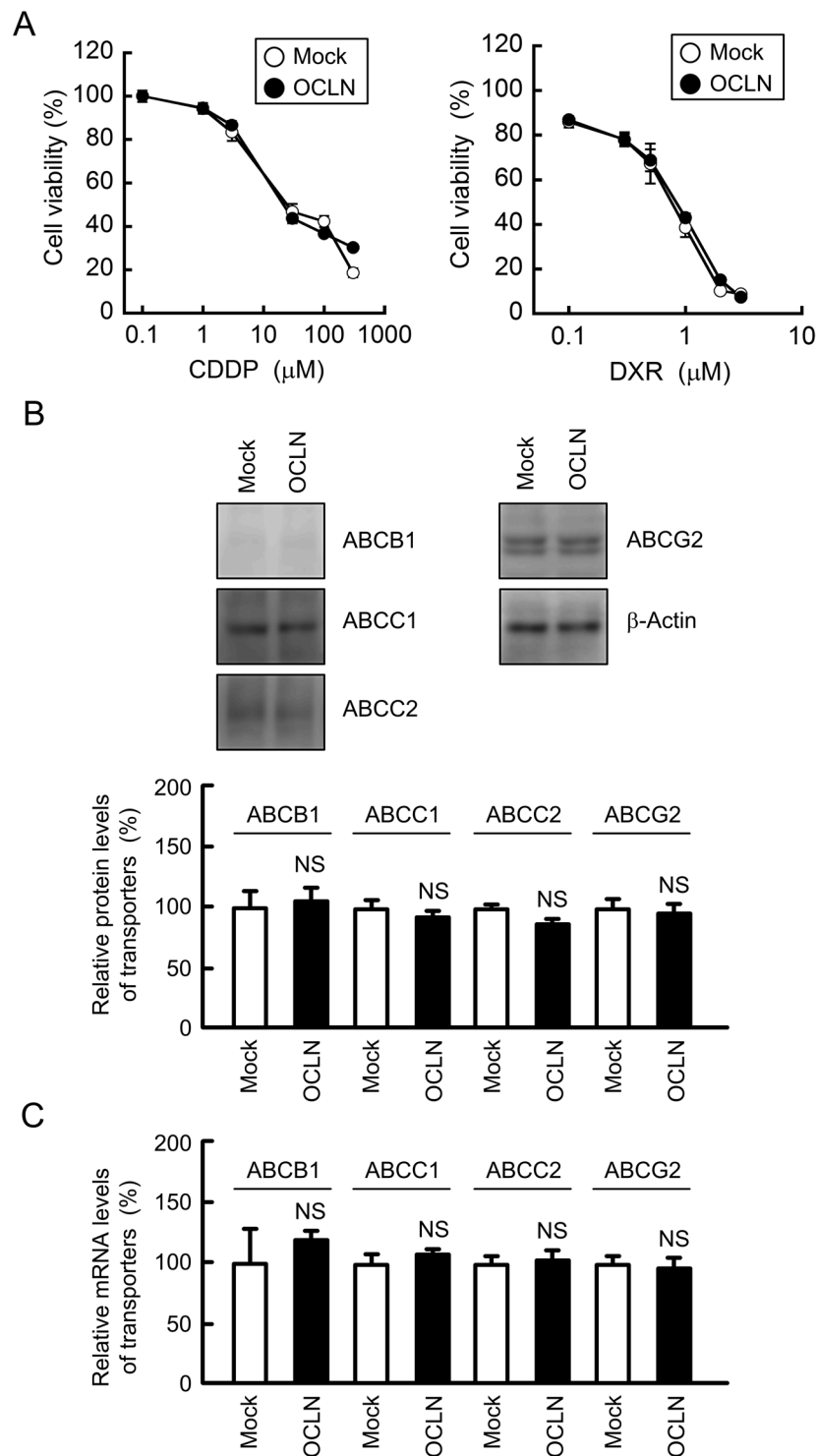


**Figure 4.** Effect of OCLN overexpression on cytotoxicity of anticancer drugs. **(A)** Mock and OCLN-expressing cells were treated with CDDP or DXR for 48 h. Cell viability was measured by WST-1 assays. **(B)** The expression of ABCB1, ABCC1, ABCC2, ABCG2, and  $\beta$ -actin in cell lysates was examined by western blotting. The protein levels of ABC transporters are shown as a percentage of the values in mock cells. The full-length blot images are shown in Supplementary Fig. S4. **(C)** The mRNA levels of ABCB1, ABCC1, ABCC2, ABCG2 are shown as a percentage of the values in mock cells.  $n = 3-6$ . NS,  $P > 0.05$  compared with mock cells.

A549/CDDP cells are greater than those in normal A549 cells (Fig. 2A). The regulatory mechanism of OCLN expression is not fully understood, but it is upregulated by a JAK-STAT3 signaling pathway in colon SW480 and HCT116 cells<sup>27</sup>. The CDDP-resistance induced elevation of OCLN expression was inhibited by LY-294002, but

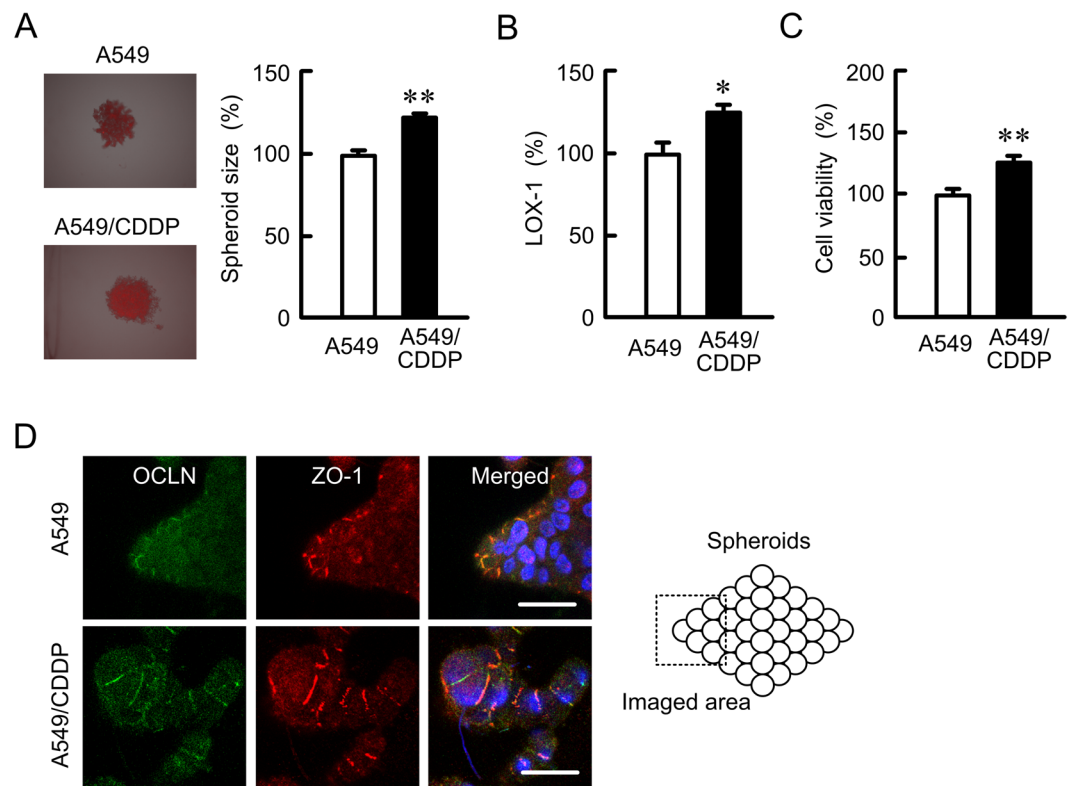


**Figure 5.** Elevation of hypoxic level and cell viability in spheroid model by CDDP resistance. (A and B) A549 and A549/CDDP cells were plated on PrimeSurface96U multi-well plates. After treating the cells with  $2\ \mu\text{M}$  LOX-1 for 24 h, the fluorescence images were acquired using a fluorescence microscope (left images). The spheroid size and fluorescence intensities of LOX-1 are represented as a percentage of the values in A549 cells. (C) The viability of spheroid cells was assessed by a CellTiter-Glo 3D Cell Viability Assay kit. (D) Immunofluorescence stainings with anti-OCLN (green) and anti-ZO-1 (red) antibodies were performed. The right images show the merged picture with DAPI (blue). Scale bar represents  $10\ \mu\text{m}$ .  $n = 4-6$ . \*\* $P < 0.01$  and \* $P < 0.05$  compared with A549.

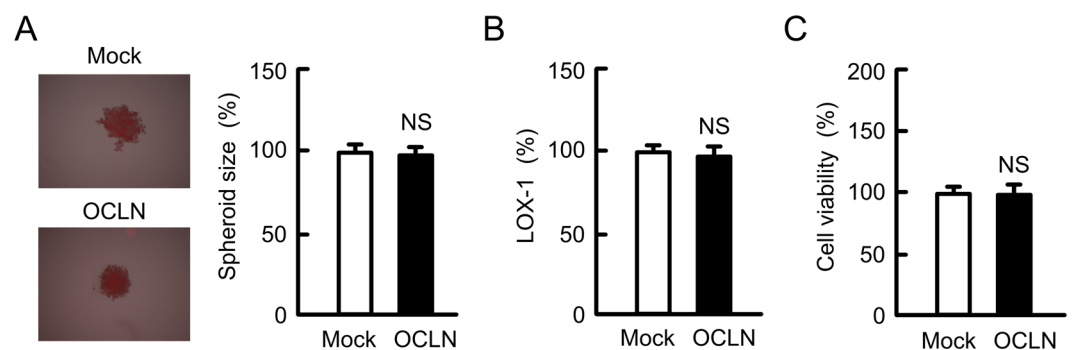


**Figure 6.** Effect of OCLN overexpression on hypoxic level and viability in spheroids. (A and B) Mock/A549, and OCLN/A549 cells were plated on PrimeSurface96U multi-well plates. After treating the cells with  $2\ \mu\text{M}$  LOX-1 for 24 h, the fluorescence images were acquired (left images). The spheroid size and fluorescence intensities of LOX-1 are represented as a percentage of the values in mock cells. (C) The viability of spheroid cells was measured.  $n = 4-6$ . NS,  $P > 0.05$  compared with mock cells.

not by U0126 (Fig. 2B,C), indicating that OCLN expression is increased by the activation of PI3K/Akt pathway in A549 cells. The upregulation mechanism of OCLN may be different in tissue types. There is a possibility that OCLN confers resistance to anticancer drugs because the expression of OCLN is regulated by a common signaling pathway with chemoresistance including ERK1/2 or Akt. However, the overexpression of OCLN in A549 cells had no effect on CDDP and DXR toxicities in 2D culture model (Fig. 4A). We recently found that CDDP resistance increases the expression level of ABCC2 in A549 cells (data not shown). In addition, the expression of ABCC2 is positively correlated with CLDN2 expression<sup>8</sup>. However, the overexpression of OCLN did not change

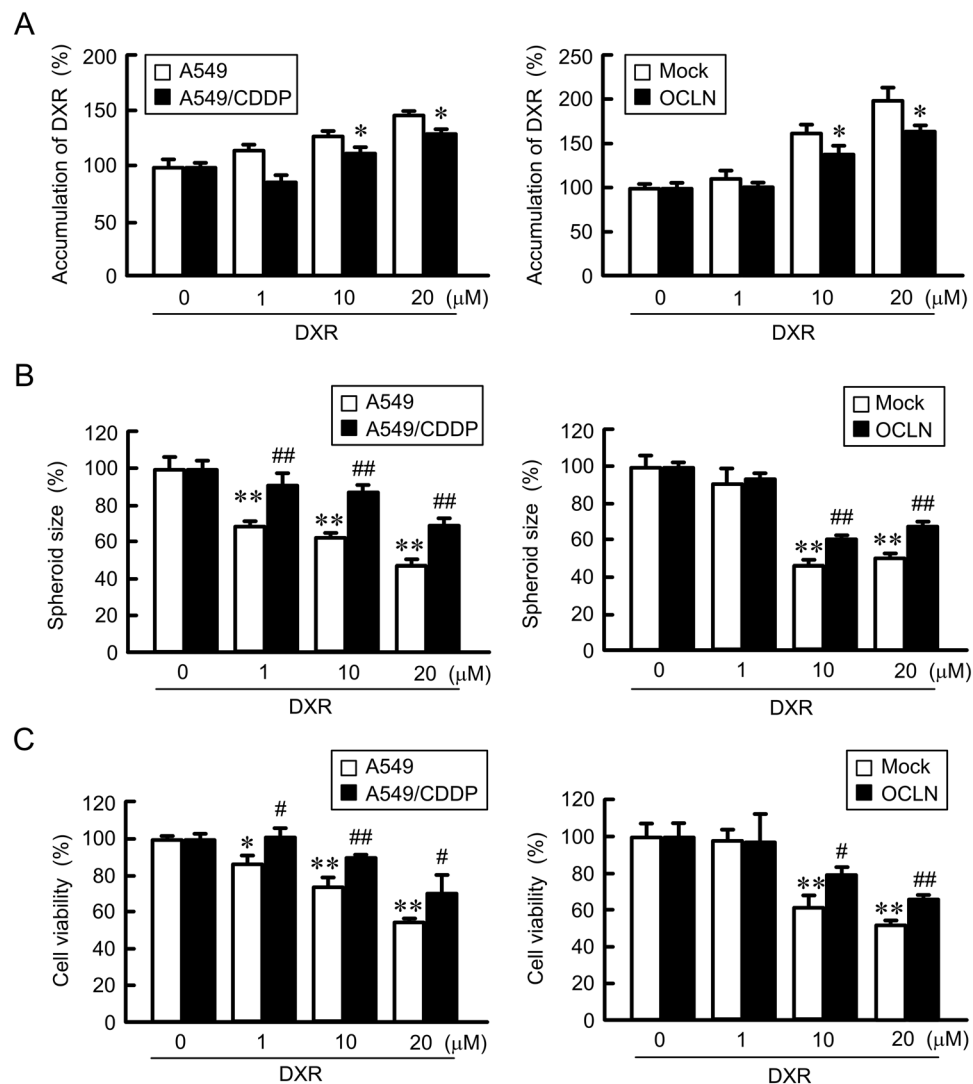


**Figure 7.** Decrease in DXR toxicity by OCLN overexpression in spheroid model. (A) A549, A549/CDDP, mock/A549, and OCLN/A549 cells were plated on PrimeSurface96U multi-well plates. The cells were incubated with DXR for 60 min. The fluorescence intensities of DXR in spheroids are shown as a percentage of 0 μM. (B and C) After treating the cells with DXR for 24 h, the spheroid size and viability of spheroid cells were measured. These values are represented as a percentage of 0 μM DXR.  $n = 3-4$ . \*\* $P < 0.01$  and \* $P < 0.05$  compared with 0 μM. \*\*\* $P < 0.01$  and \*\* $P < 0.05$  compared with 0 μM. ## $P < 0.01$  and # $P < 0.05$  compared with A549 or mock.

the protein and mRNA levels of ABC transporters including ABCC2 (Fig. 4B,C). The overexpression of OCLN is suggested not to be directly implicated in the acquisition of chemoresistance in A549 cells.

The properties of paracellular permeability to larger molecules are also characterized by CLDNs. The activation of checkpoint kinase 1 decreases paracellular permeability to fluorescein isothiocyanate-dextran (MW: 4 kDa, FD-4) mediated via the elevation of CLDN5 in Caco-2 and T84 cells<sup>28</sup>. The knockdown of CLDN2 by siRNA decreases the paracellular flux of urea (MW: 60) in Caco-2 and renal tubular MDCK II cells<sup>29</sup>. We recently reported that paracellular permeability to lucifer yellow (LY, MW: 457), a tracer for paracellular transport, was increased by CLDN2 knockdown in A549 cells<sup>8</sup>. Few reports show that OCLN is also implicated in the regulation of paracellular transport of larger molecules. Knockdown of OCLN expression by siRNA increases transepithelial flux of urea (MW: 60), mannitol (MW: 182), inulin (MW: 5,000), and dextran (MW: 10,000 and 70,000) in Caco-2 cells<sup>30</sup>. Similarly, internalization of OCLN increases paracellular permeability to FD-4 in Caco-2 cells<sup>31</sup> and LY in mouse MCE301 cells<sup>32</sup>. We found that OCLN overexpression significantly suppresses paracellular permeability to DXR (MW: 543) in A549 cells. OCLN may function as paracellular barrier to large molecules in chemoresistant lung adenocarcinoma cells.

Paracellular permeability to DXR was suppressed by CDDP-resistance, which were recovered by LY-294002 without affecting TER (Fig. 3A,B). These results suggest that OCLN may not be essential to regulate paracellular permeability to ions, but we cannot deny the involvement of other CLDNs. Actually, the expression of CLDN1 was also elevated by CDDP-resistance in A549 cells, which was blocked by LY-294002<sup>9</sup>. The balance of the expression of CLDNs and OCLN may induce this property of paracellular permeability to ions. However, our data



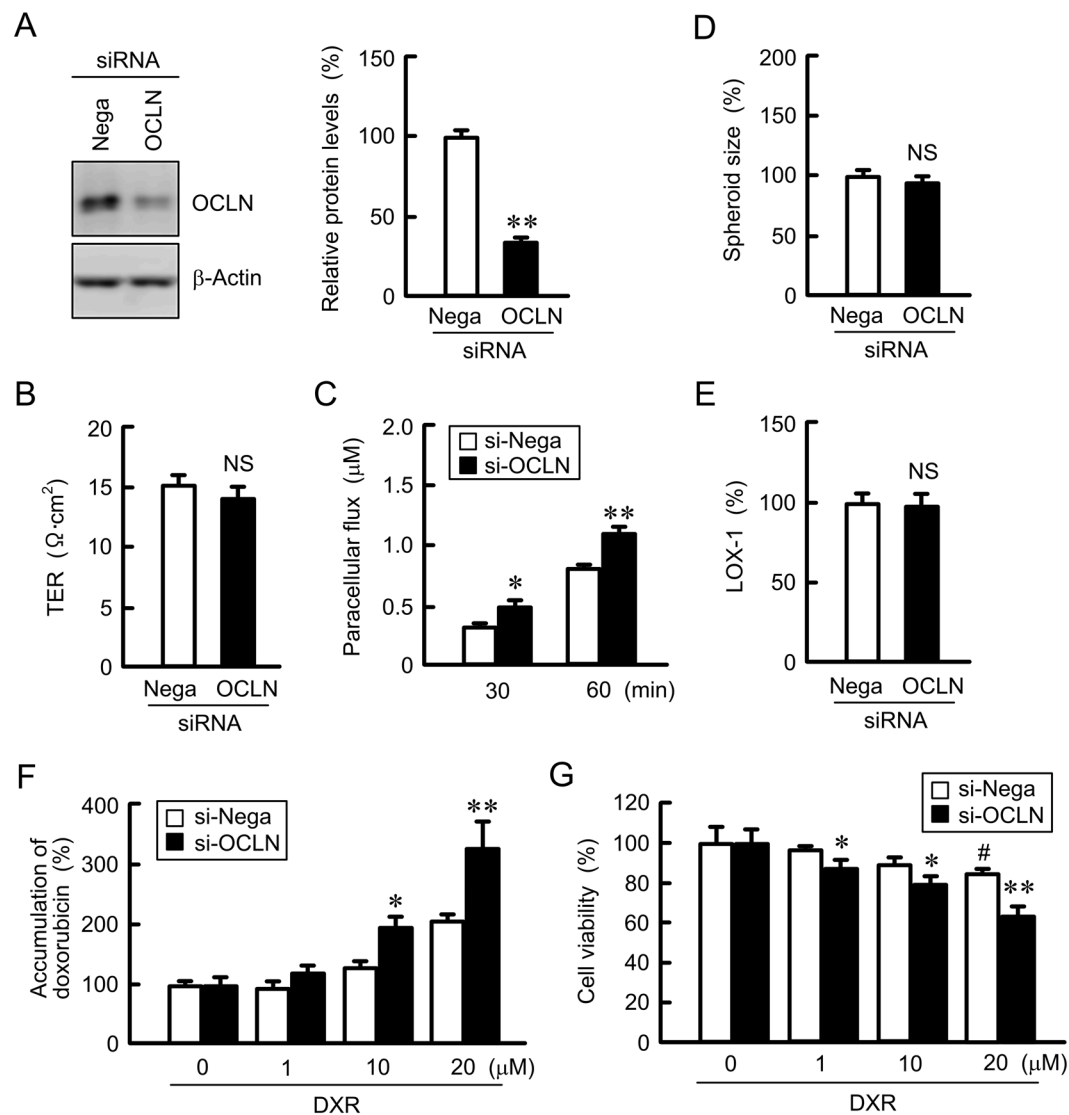


**Figure 8.** Increase in DXR toxicity by *OCLN* siRNA in spheroid model. (A) The expression of *OCLN* and  $\beta$ -actin in A549/CDDP cells transfected with negative (Nega) or *OCLN* siRNA were examined by western blotting. The protein levels of *OCLN* are shown as a percentage of the values in negative siRNA. The full-length blot images are shown in Supplementary Fig. S5. (B) TER was measured in negative and *OCLN* siRNA-transfected A549/CDDP cells. (C) Paracellular DXR flux for 30 and 60 min was measured in negative and *OCLN* siRNA-transfected A549/CDDP cells. (D and E) A549/CDDP cells transfected with negative or *OCLN* siRNA were plated on PrimeSurface96U multi-well plates. The spheroid size and fluorescence intensity of LOX-1 are represented as a percentage of the values in negative siRNA. (F) Negative and *OCLN* siRNA-transfected A549/CDDP cells were incubated with DXR for 60 min at the concentrations indicated. The fluorescence intensities of DXR in spheroids are shown as a percentage of 0  $\mu$ M. (G) Negative and *OCLN* siRNA-transfected A549/CDDP cells were incubated with DXR for 24 h at the concentrations indicated. The viability of spheroid cells was assessed.  $n = 3-4$ . \*\* $P < 0.01$  and \* $P < 0.05$  compared with negative siRNA. ## $P < 0.01$  and # $P < 0.05$  compared with 0  $\mu$ M DXR. NS,  $P > 0.05$  compared with negative siRNA.

(Fig. 3D) and other reports<sup>33</sup> strongly support that *OCLN* is not implicated in the regulation of paracellular ion flux. Few reports demonstrate that TER is changed by a decrease in *OCLN* expression<sup>34</sup>, which may be indirectly caused by the change of CLDNs expression or interaction with an adaptor protein, ZO-1.

The microenvironment formed by tumor cells in the body could be a cause of drug resistance. The hypoxic level was increased in A549/CDDP cells compared to A549 cells (Fig. 5), suggesting that A549/CDDP cells are exposed to more severe hypoxic environment compared to A549 cells. In contrast, the hypoxic level and viability in A549/*OCLN* cells were similar to those in mock cells (Fig. 6). The correlation between junctional proteins and the formation of stress environments in spheroids are not fully understood. In immunofluorescence measurement of spheroid cells showed that both *OCLN* and ZO-1 are distributed in the cell-cell border area of most outside cells (Fig. 5D). We suggest that *OCLN* is not directly implicated in the formation of hypoxic environment in A549 spheroid cells. Conversely, the sensitivity against anticancer drugs was influenced by overexpression and

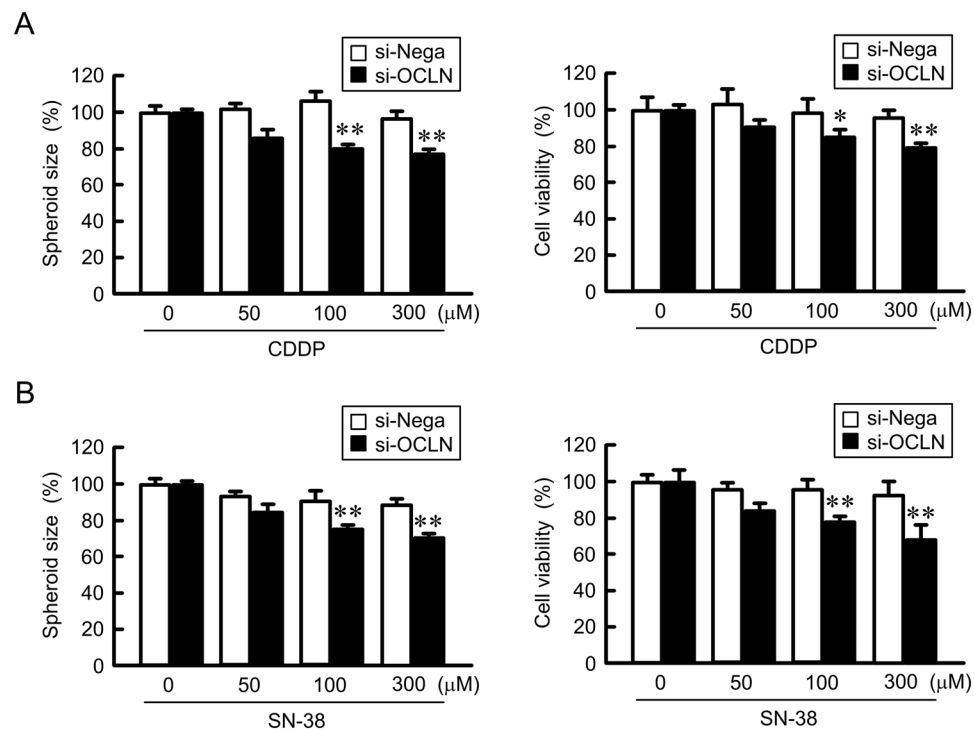


**Figure 9.** Enhancement of chemosensitivity by OCLN knockdown in A549/CDDP spheroid cells. Negative control or *OCLN* siRNAs were transfected in A549/CDDP cells. After 48 h of transfection, the cells were treated with CDDP (A) or SN-38 (B) for additional 48 h. The size and cell viability of spheroids are shown as a percentage of negative siRNA.  $n = 3-4$ . \*\* $P < 0.01$  and \* $P < 0.05$  compared with negative siRNA.

knockdown of *OCLN* (Figs 7–9). These results suggest that *OCLN* enhances chemoresistance mediated through blocking of accumulation of anticancer drugs in spheroids.

Taken together, *OCLN* expression was elevated by CDDP resistance mediated through the activation of Akt in A549 cells. *OCLN* expression was also induced by resistance to DXR, SN-38, and GEM in A549 cells, and resistant to CDDP in RERF-LC-MS and PC-3 cells. The overexpression of *OCLN* inhibited the paracellular DXR flux in 2D monolayers, but did not change chemoresistance. In contrast, the anticancer drug-induced toxicities were enhanced by *OCLN* knockdown in A549/CDDP spheroid cells. *OCLN* may be not directly implicated in the acquisition of resistance to anticancer drugs in lung adenocarcinoma cells, but it suppresses chemosensitivity in spheroid cells. Our recent data indicate that *CLDN1* and *CLDN2* are also implicated in the development of chemoresistance in 3D spheroid cells<sup>8,9</sup>. These tight junctional proteins may be new targets of adjuvant chemotherapy in lung adenocarcinoma.

## Material and Methods

**Materials.** Mouse anti-ZO-1 monoclonal antibody (33–9100, Lot: 1100420A) and Lipofectamine 2000 were obtained from Thermo Fisher Scientific (Rockford, IL, USA). Rabbit anti-p-Akt (4060, Lot: 14), anti-Akt (4691, Lot: 20), anti-p44/42 MAPK (ERK1/2, 4695, Lot: 1), anti-c-Fos (2250, Lot: 4), and anti-MRP2 (ABCC2, 4446, Lot: 1) polyclonal antibodies were from Cell Signaling Technology (Beverly, MA, USA). Goat anti- $\beta$ -actin (sc-1615, Lot: C141), rabbit anti-p-ERK1/2 (sc-16982R, Lot: L0704) polyclonal antibodies and mouse anti-p-c-Fos (sc-81485, E2008) monoclonal antibodies were from Santa Cruz Biotechnology (Santa Cruz, CA, USA). Rabbit anti-ABCB1 (GTX108354, Lot: 39834), anti-ABCC1 (GTX116046, Lot: 40135), and anti-ABCG2 (GTX100437, Lot: 39471) polyclonal antibodies were from GeneTex (Irvine, CA, USA). Mouse anti-FLAG (018-22381, Lot: SAQ1191) monoclonal antibody, CDDP, and DXR were from Wako Pure Chemical (Osaka, Japan). LY-294002, and U0126 were purchased from BIOMOL Research Laboratories (Plymouth Meeting, PA, USA) and Sigma-Aldrich (Saint Louis, MO, USA), respectively. All other reagents were of the highest purity commercially available.

**Cell culture.** A549 cells derived from human lung adenocarcinoma were obtained from the RIKEN BRC through the National Bio-Resource Project of the MEXT (Ibaraki, Japan). Human lung adenocarcinoma RERF-LC-MS (JCRB0081) and PC-3 (JCRB0077) cells were obtained from the JCRB Cell Bank (National Institute of Health Sciences, Tokyo, Japan). The cells were grown in Dulbecco's modified Eagle's medium (DMEM, Sigma-Aldrich) supplemented with 5% fetal calf serum (FCS, HyClone, Logan, UT, USA), 0.07 mg/ml penicillin-G potassium, and 0.14 mg/ml streptomycin sulfate in a 5% CO<sub>2</sub> atmosphere at 37 °C.

**Plasmid DNA construction and transfection.** Flag-tagged *OCLN* vector (#86042) was purchased from Addgene (Cambridge, MA, USA). The *OCLN* cDNA was subcloned into pTRE2-hyg vector (Clontech

Genes	Direction	Sequence
<i>OCN</i>	Sense	5'-TTGTGGGACAAGGAACACA-3'
<i>OCN</i>	Antisense	5'-TCATTCACTTGCCATTGGA-3'
<i>ABCB1</i>	Sense	5'-CCCATCATTGCAATAGCAGG-3'
<i>ABCB1</i>	Antisense	5'-TGTTCAAACCTCTGCTCCTGA-3'
<i>ABCC1</i>	Sense	5'-ATGTCACGTGGAATACCAGC-3'
<i>ABCC1</i>	Antisense	5'-GAAGACTGAACTCCCTTCCT-3'
<i>ABCC2</i>	Sense	5'-ACAGAGGCTGGTGGCAACC-3'
<i>ABCC2</i>	Antisense	5'-ACCATTACCTTGTCACCTGTCATGA-3'
<i>ABCG2</i>	Sense	5'-AGATGGGTTTCCAAGCGTTCAT-3'
<i>ABCG2</i>	Antisense	5'-CCAGTCCCAGTACGACTGTGACA-3'
$\beta$ -Actin	Sense	5'-CCTGAGGCACTTCCAGCCTT-3'
$\beta$ -Actin	Antisense	5'-TGCGGATGTCCACGTCACACTTC-3'

**Table 1.** Primers for real time PCR.

Laboratories, Mountain View, CA, USA). The siRNAs for negative control and *OCN* were purchased from Santa Cruz and Sigma-Aldrich, respectively. Mock (empty vector), *OCN*/pTRE2 vector, or siRNA was transfected into cells using Lipofectamine 2000 as recommended by the supplier. Stable transfectants of mock and *OCN* were selected with 400  $\mu$ g/ml hygromycin B and picked with a ring clone. Subsequently the cells were subsequently maintained in the presence of 50  $\mu$ g/ml hygromycin B. To establish resistant cells against CDDP, DXR, SN-38, and GEM, A549 cells were continuously cultured in the growth medium supplemented with these anticancer drugs, whose concentration was increased in a stepwise manner (CDDP: 1, 2, 3, 4, and 5  $\mu$ M; DXR: 1, 5, 10, 15, and 20 nM; SN-38: 10, 20, 30, 40, and 50 nM; GEM: 1, 2, 3, 4 and 5 nM) for 4–6 weeks. The established resistant cells were maintained in the growth medium containing 5  $\mu$ M CDDP, 20 nM DXR, 50 nM SN-38, or 5 nM GEM. The cell growth was completely inhibited at higher concentration of anticancer drugs. Similarly we obtained CDDP-resistant RERF-LC-MS and PC-3 cells.

**3D culture spheroid model.** Cells were plated at densities of  $1 \times 10^4$  cells/well on PrimeSurface96U multi-well plates (Sumitomo Bakelite, Tokyo, Japan). After culturing for 96 h, the size and viability of spheroids were measured as described previously<sup>9</sup>. The fluorescence intensities of DXR and LOX-1, a hypoxia probe, were calculated using ImageJ software.

**Cytotoxicity of anticancer drugs.** Cells were plated on 96-well flat bottomed plates or PrimeSurface96U multi-well plates. Anticancer drugs were applied for 24 h in FCS-free media. In 2D and 3D culture models, the cell viability was measured using a Premix WST-1 Cell Proliferation Assay Kit (Takara, Otsu, Japan) and a CellTiter-Glo 3D Cell Viability Assay kit (Promega, Madison, WI, USA), respectively.

**Isolation of total RNA and quantitative real time PCR.** Total RNA was extracted using TRI reagent (Sigma-Aldrich). Reverse transcription and quantitative real time PCR was performed as described previously<sup>35</sup>. The primer pairs used for PCR are listed in Table 1.

**Sodium dodecyl sulfate (SDS)-polyacrylamide gel electrophoresis and western blotting.** Confluent A549 cells were scraped into cold phosphate-buffered saline and precipitated by centrifugation. Then, the cells were lysed in a RIPA buffer (150 mM NaCl, 50 mM Tris-HCl (pH8.0), 1% Triton X-100, 0.1% SDS, 0.5 mM EDTA) supplemented with a protease inhibitor cocktail (Sigma-Aldrich), and sonicated for 20 s. The lysates were used as whole cell extracts. After centrifugation at 6,000  $\times$  g for 5 min, the resultant supernatants which include membrane and cytoplasmic proteins were used as cell lysates. SDS-polyacrylamide gel electrophoresis and western blotting were carried out as described previously<sup>9</sup>.

**Confocal microscopy.** Cells were plated on cover glasses. After forming confluent monolayer, the cells were incubated with 4% paraformaldehyde for 15 min at 4 °C and then permeabilized with 0.2% Triton X-100 for 15 min. Following permeabilization, the cells were blocked with 4% Block Ace (Dainippon Sumitomo Pharma, Osaka, Japan) for 30 min and incubated with anti-OCN (1:100 dilution) and anti-ZO-1 (1:100 dilution) antibodies for 16 h at 4 °C. They were then incubated with Alexa Fluor 488- and 555-conjugated antibodies (1:100 dilution) for 1.5 h at room temperature. In 3D culture model, the cells plated on PrimeSurface96U multi-well plates were cultured for 96 h. Following incubation with 4% paraformaldehyde for 30 min, the cells were permeabilized with 0.2% Triton X-100 for 30 min. After blocking with Block Ace, they were stained with anti-OCN (1:100 dilution) and anti-ZO-1 (1:100 dilution) antibodies for 16 h at 4 °C, followed by incubation with secondary antibodies as described above. For transparency, the samples were treated with Visikol-HISTO-M (Visikol, Whitehouse Station, NJ, USA). The fluorescence images were observed using an LSM 700 confocal microscope (Carl Zeiss, Jena, Germany).

**Measurement of paracellular permeability.** Cells were plated at densities of  $5 \times 10^4$  cells on transwell plates (0.4  $\mu$ m pore size, Corning Incorporated, Corning, NY, USA). After forming confluent monolayer, TER and paracellular permeability to DXR were measured as described previously<sup>9</sup>.

**Statistical analysis.** All experiments were performed using at least 3 independent samples. Data are presented as means  $\pm$  standard errors of mean. Analysis between two groups was done using Student's *t* test. For comparison between multiple groups, one-way analysis (ANOVA) followed by Tukey's multiple comparison test was used. Statistical analysis was performed with KaleidaGraph version 4.5.1 software (Synergy Software, PA, USA). *p* value < 0.05 was considered to be statistically significant.

## References

1. Miller, K. D. *et al.* Cancer treatment and survivorship statistics, 2016. *CA Cancer J. Clin.* **66**, 271–289 (2016).
2. Castells, M., Thibault, B., Delord, J. P. & Couderc, B. Implication of tumor microenvironment in chemoresistance: tumor-associated stromal cells protect tumor cells from cell death. *International journal of molecular sciences* **13**, 9545–9571 (2012).
3. Kartal-Yandim, M., Adan-Gokbulut, A. & Baran, Y. Molecular mechanisms of drug resistance and its reversal in cancer. *Crit. Rev. Biotechnol.* **36**, 716–726 (2016).
4. Senthane, D. A. *et al.* The Role of Tumor Microenvironment in Chemoresistance: To Survive, Keep Your Enemies Closer. *International journal of molecular sciences* **18** (2017).
5. Phung, Y. T., Barbone, D., Broaddus, V. C. & Ho, M. Rapid generation of *in vitro* multicellular spheroids for the study of monoclonal antibody therapy. *J. Cancer* **2**, 507–514 (2011).
6. Longati, P. *et al.* 3D pancreatic carcinoma spheroids induce a matrix-rich, chemoresistant phenotype offering a better model for drug testing. *BMC Cancer* **13**, 95 (2013).
7. Torisawa, Y. S., Shiku, H., Yasukawa, T., Nishizawa, M. & Matsue, T. Multi-channel 3-D cell culture device integrated on a silicon chip for anticancer drug sensitivity test. *Biomaterials* **26**, 2165–2172 (2005).
8. Maruhashi, R. *et al.* Elevation of sensitivity to anticancer agents of human lung adenocarcinoma A549 cells by knockdown of claudin-2 expression in monolayer and spheroid culture models. *Biochim. Biophys. Acta* **1865**, 470–479 (2018).
9. Akizuki, R. *et al.* Decrease in paracellular permeability and chemosensitivity to doxorubicin by claudin-1 in spheroid culture models of human lung adenocarcinoma A549 cells. *Biochim. Biophys. Acta* **1865**, 769–780 (2018).
10. Tsukita, S., Yamazaki, Y., Katsuno, T. & Tamura, A. Tight junction-based epithelial microenvironment and cell proliferation. *Oncogene* **27**, 6930–6938 (2008).
11. Powell, D. W. Barrier function of epithelia. *Am. J. Physiol. Gastrointest. Liver Physiol.* **241**, G275–G288 (1981).
12. Matter, K. & Balda, M. S. Signalling to and from tight junctions. *Nat. Rev. Mol. Cell Biol.* **4**, 225–236 (2003).
13. Wittchen, E. S., Haskins, J. & Stevenson, B. R. Protein interactions at the tight junction. Actin has multiple binding partners, and ZO-1 forms independent complexes with ZO-2 and ZO-3. *J. Biol. Chem.* **274**, 35179–35185 (1999).
14. Furuse, M. Molecular basis of the core structure of tight junctions. *Cold Spring Harb. Perspect. Biol.* **2**, a002907 (2010).
15. Riazuddin, S. *et al.* Tricellulin is a tight-junction protein necessary for hearing. *Am. J. Hum. Genet.* **79**, 1040–1051 (2006).
16. Mineta, K. *et al.* Predicted expansion of the claudin multigene family. *FEBS Lett.* **585**, 606–612 (2011).
17. Turksen, K. & Troy, T. C. Barriers built on claudins. *J. Cell Sci.* **117**, 2435–2447 (2004).
18. Furuse, M. *et al.* Occludin: a novel integral membrane protein localizing at tight junctions. *J. Cell Biol.* **123**, 1777–1788 (1993).
19. Wang, F. *et al.* Heterogeneity of claudin expression by alveolar epithelial cells. *Am. J. Respir. Cell Mol. Biol.* **29**, 62–70 (2003).
20. Chapman, K. E., Waters, C. M. & Miller, W. M. Continuous exposure of airway epithelial cells to hydrogen peroxide: protection by KGF. *J. Cell. Physiol.* **192**, 71–80 (2002).
21. Tobioka, H. *et al.* Expression of occludin, a tight-junction-associated protein, in human lung carcinomas. *Virchows Arch.* **445**, 472–476 (2004).
22. Paschoud, S., Bongiovanni, M., Pache, J. C. & Citi, S. Claudin-1 and claudin-5 expression patterns differentiate lung squamous cell carcinomas from adenocarcinomas. *Mod. Pathol.* **20**, 947–954 (2007).
23. Kuo, W. T., Tu, D. G., Chiu, L. Y., Sheu, G. T. & Wu, M. F. High pemetrexed sensitivity of docetaxel-resistant A549 cells is mediated by TP53 status and downregulated thymidylate synthase. *Oncol. Rep.* **38**, 2787–2795 (2017).
24. Wang, W. *et al.* Establishment and biological characteristics of a multi-drug resistant cell line A549/Gem. *Zhongguo Fei Ai Za Zhi* **11**, 55–61 (2008).
25. Fu, X. *et al.* PAK4 confers cisplatin resistance in gastric cancer cells via PI3K/Akt- and MEK/ERK-dependent pathways. *Biosci. Rep.* **34** (2014).
26. Yoon, H., Min, J. K., Lee, J. W., Kim, D. G. & Hong, H. J. Acquisition of chemoresistance in intrahepatic cholangiocarcinoma cells by activation of AKT and extracellular signal-regulated kinase (ERK)1/2. *Biochem. Biophys. Res. Commun.* **405**, 333–337 (2011).
27. Xue, J. *et al.* LncRNA AB073614 induces epithelial-mesenchymal transition of colorectal cancer cells via regulating the JAK/STAT3 pathway. *Cancer Biomark* (2018).
28. Hering, N. A. *et al.* Transforming growth factor-beta, a whey protein component, strengthens the intestinal barrier by upregulating claudin-4 in HT-29/B6 cells. *J. Nutr.* **141**, 783–789 (2011).
29. Nighot, P. K., Hu, C. A. & Ma, T. Y. Autophagy enhances intestinal epithelial tight junction barrier function by targeting claudin-2 protein degradation. *J. Biol. Chem.* **290**, 7234–7246 (2015).
30. Al-Sadi, R. *et al.* Occludin regulates macromolecule flux across the intestinal epithelial tight junction barrier. *Am. J. Physiol. Gastrointest. Liver Physiol.* **300**, G1054–1064 (2011).
31. Yamaki, T. *et al.* A mechanism enhancing macromolecule transport through paracellular spaces induced by Poly-L-Arginine: Poly-L-Arginine induces the internalization of tight junction proteins via clathrin-mediated endocytosis. *Pharm. Res.* **31**, 2287–2296 (2014).
32. Manabe, A. *et al.* Chlorpheniramine Increases Paracellular Permeability to Marker Fluorescein Lucifer Yellow Mediated by Internalization of Occludin in Murine Colonic Epithelial Cells. *Biol. Pharm. Bull.* **40**, 1299–1305 (2017).
33. Yu, A. S. *et al.* Knockdown of occludin expression leads to diverse phenotypic alterations in epithelial cells. *Am. J. Physiol. Cell Physiol.* **288**, C1231–1241 (2005).
34. Thakre-Nighot, M. & Blikslager, A. T. Indomethacin induces increase in gastric epithelial tight junction permeability via redistribution of occludin and activation of p38 MAPK in MKN-28 Cells. *Tissue barriers* **4**, e1187325 (2016).
35. Ikari, A., Sato, T., Watanabe, R., Yamazaki, Y. & Sugatani, J. Increase in claudin-2 expression by an EGFR/MEK/ERK/c-Fos pathway in lung adenocarcinoma A549 cells. *Biochim. Biophys. Acta* **1823**, 1110–1118 (2012).

## Acknowledgements

This work was supported in part by JSPS KAKENHI Grant Number 15H04657 and grants from the Takahashi Sangyo-Keizai Research Foundation, Takeda Science Foundation, Smoking Research Foundation, and Futaba Electronics Memorial Foundation (to A.I.).

### Author Contributions

H.E., R.A. and R.M. conducted experiments and analyzed the data. M.T., T.F., T.M. and S.E. contributed to the experiment plan and discussion of the manuscript. A.I. supervised the project, interpretation of data, and writing the paper. All authors reviewed the results and approved the final version of the manuscript.

### Additional Information

**Supplementary information** accompanies this paper at <https://doi.org/10.1038/s41598-018-33566-w>.

**Competing Interests:** The authors declare no competing interests.

**Publisher's note:** Springer Nature remains neutral with regard to jurisdictional claims in published maps and institutional affiliations.



**Open Access** This article is licensed under a Creative Commons Attribution 4.0 International License, which permits use, sharing, adaptation, distribution and reproduction in any medium or format, as long as you give appropriate credit to the original author(s) and the source, provide a link to the Creative Commons license, and indicate if changes were made. The images or other third party material in this article are included in the article's Creative Commons license, unless indicated otherwise in a credit line to the material. If material is not included in the article's Creative Commons license and your intended use is not permitted by statutory regulation or exceeds the permitted use, you will need to obtain permission directly from the copyright holder. To view a copy of this license, visit <http://creativecommons.org/licenses/by/4.0/>.

© The Author(s) 2018